Appl. Sci. Converg. Technol. 30 (5); 152-155 (2021)
https://doi.org/10.5757/ASCT.2021.30.5.152
eISSN: 2288-6559

Research Paper Check for updates

Effect of Reaction Time on Optical Properties of $CsPbBr_3$ Perovskite Nanocrystals

Received 8 July, 2021; revised 1 August, 2021; accepted 4 August, 2021

Sung Hun Kim[a], Yong-Ryun Jo[b], Yong Bin Kim[a,b], Ju Seok Kim[a], Sang-Youp Yim[b], and Hong Seok Lee[a,*]

[a]Department of Physics, Research Institute of Physics and Chemistry, Jeonbuk National University, Jeonju 54896, Republic of Korea
[b]Advanced Photonics Research Institute, Gwangju Institute of Science and Technology, Gwangju 61005, Republic of Korea

*Corresponding author E-mail: hslee1@jbnu.ac.kr

ABSTRACT

We have studied the optical and structural properties of $CsPbBr_3$ perovskite nanocrystals (NCs) fabricated with various reaction times. The temporal evolution of the ensemble optical properties, such as absorption and fluorescence (FL) spectra and photoluminescence quantum yield (PLQY), was recorded under a set reaction temperature (170 °C) and various amounts of time (5 s – 60 min). The FL intensity of the $CsPbBr_3$ NCs gradually decreased with increasing reaction time, and the observed PLQY of the $CsPbBr_3$ NCs ranged from less than 20% up to 35% because of the enlarged crystal size and the induced charge trap states. The FL peaks of as-obtained $CsPbBr_3$ NCs were tuned in the range of 516.8 to 526.8 nm with increasing reaction time as a result of the ripening phenomenon. Transmission electron microscopy and selected area electron diffraction analysis were performed to analyze the structural properties. The results revealed that the average edge length of $CsPbBr_3$ NCs with a reaction time of 5 s was 13.4 nm and confirmed that the cubic crystal structure was well ordered.

Keywords: Perovskite nanocrystals, $CsPbBr_3$, Reaction time, Optical properties, Photoluminescence quantum yield

1. Introduction

All-inorganic cesium lead halide perovskite nanocrystals (NCs) have attracted significant attention because they demonstrate higher tolerance compared to organic-inorganic perovskites such as $CH_3NH_3PbX_3$ NCs in applications such as light-emitting diodes and solar cells [1, 2]. $CH_3NH_3PbX_3$ perovskites are also strongly associated with autodegradation because of their intrinsic instabilities [3]. So it is necessary to realize an efficient strategy for solving these problems. The thermal durability of organic-inorganic perovskites is regarded as one of the most critical issues for solar cell performance [4]. Perovskite materials are vulnerable to damage during thermal annealing, and heat dissipation is known to have an influence on perovskites, which results in thermal-induced mechanical stress and structural evolution within the NCs [5]. In organic-inorganic hybrid perovskites, the occurrence of a structural phase transition is correlated with its own characteristics and the contents of ambient air, temperature, and pressure, which have an effect on the durability of perovskite solar cells [6]. Replacement of the methylammonium (MA) cation with the less active cation of Cs can allow $CsPbBr_3$ NCs to exhibit superior thermal stability, chemical durability, and striking optical properties [7, 8]. The purpose of substituting MA cation is to form a more stable cubic phase, along with the appropriate modulation of the conduction band of the perovskite, which is the key feature to achieve stability [9]. Therefore, tailoring the optical properties of $CsPbBr_3$ NCs to make them more suitable for application is a promising approach [10]. $CsPbBr_3$ NCs can be fabricated employing a method in which oleylamine (OAm) and oleic acid (OA) are used as capping agents. The carboxylate and amine functional groups of OA and OAm are attached to the surface of the NCs during the reaction, resulting in the stability of the NCs. These long-chain hydrocarbon ligands promote the dispersion of $CsPbBr_3$ NCs in various organic media [11]. In particular, to fulfill the requirements for optoelectronic devices, the optical properties, growth stage, morphology, and structure of $CsPbBr_3$ NCs should be regulated during reproducible preparation, and various challenges in the synthetic strategy should be addressed [12].

To obtain more insight into this process, we here report the optical properties of $CsPbBr_3$ perovskite NCs fabricated with various reaction times. The UV-vis absorption and fluorescence (FL) measurements were conducted with a focus on the deterioration of the optical properties of the $CsPbBr_3$ NCs. Significant changes were also observed in the photoluminescence quantum yield (PLQY) of the $CsPbBr_3$ NCs with various reaction times. In addition, the single-crystalline cubic-phase $CsPbBr_3$ NCs and their size distributions were determined via field-emission transmission electron microscopy (FETEM).

2. Experimental details

For the preparation of Cs-oleate, Cs_2CO_3 (0.391 g, 1.2 mmol), OA (1.27 mL, 4 mmol), and 1-octadecene (18.73 mL) were loaded into a 100 mL three-neck flask and vacuumed for 1 h at 120 °C. Then, the mixture was reacted at 160 °C under flowing N_2 gas until the precursor solution was completely dissolved. Because Cs-oleate precipitates out of 1-octadecene at room temperature, it needs to be preheated to 100 °C before use. Next, for the synthesis of $CsPbBr_3$ NCs with various reaction times, $PbBr_2$ (0.149 g, 4 mmol) and 1-octadecene (18.73 mL) were placed in a 100 mL three-neck flask and vacuumed for 1 h at 120 °C, after which OA (1 mL) and OAm (3 mL) were injected at 120 °C. After $PbBr_2$ was completely solubilized, the mixture was heated

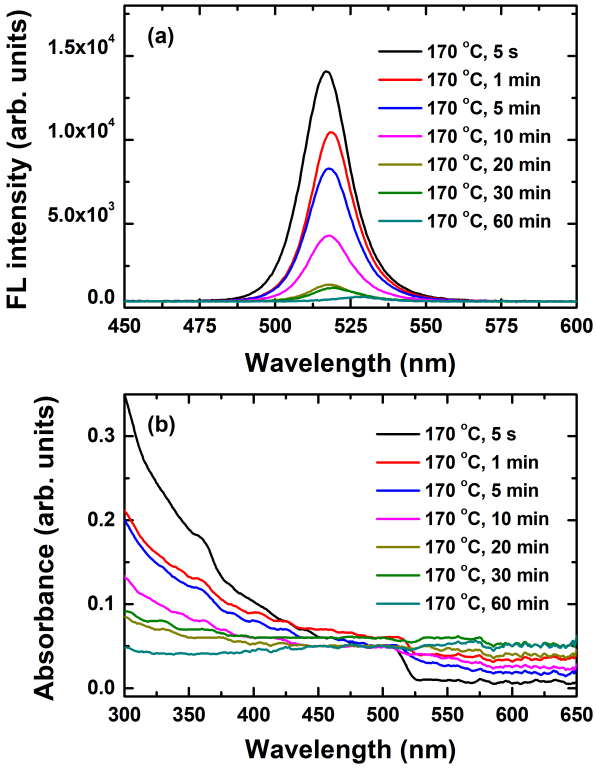

Figure 1. (a) Fluorescence and (b) absorption spectra of $CsPbBr_3$ nanocrystals with various reaction times.

up to 170 °C, and 2 mL of the Cs-oleate stock solution was injected swiftly into the reaction system. Subsequently, the sample was obtained after a set reaction time (5 s, 1, 5, 10, 20, 30, and 60 min). Then, the reaction mixture was cooled down with an ice-water bath. The resulting mixture was precipitated with *tert*-butanol by centrifugation at 7,000 rpm for 10 min. After centrifugation, the supernatant was eliminated, and the resulting precipitate was obtained. The resulting precipitate was re-dispersed in toluene for UV-vis and TEM measurements. UV-vis absorption and FL measurements of the $CsPbBr_3$ NCs were performed using a FLAME-S spectrophotometer (Ocean Optics Inc., Largo, FL, USA) at room temperature. The crystalline structure, morphology and size distributions of the $CsPbBr_3$ NCs were investigated by using a FETEM (Tecnai G^2, F30 S-Twin, 300 keV, Thermo Fisher Scientific, Waltham, MA, USA).

3. Results and discussion

The FL and absorption spectra of $CsPbBr_3$ NCs with various reaction times are shown in Fig. 1. The crystallite growth of $CsPbBr_3$ NCs in solution primarily depends on the LaMer mechanism [13]. The growth stage of the $CsPbBr_3$ NCs can be divided into three distinct phases, i.e., the nucleation, growth, and regrowth processes. The hot-injection in wet chemical route for colloidal synthesis of the $CsPbBr_3$ NCs has benefits with respect to controlling particle size and size distribution [14]. At 5 s of reaction time, the $CsPbBr_3$ NCs showed a sharp absorption and a narrow emission peak. The full-width at half-maximum for the $CsPbBr_3$ NCs was 20.2, 18.6, 19.3, 18.8, 18.7, 19.9, and 20.3 nm for reaction times of 5 s, 1, 5, 10, 20, 30, and 60 min, respectively. As the reaction time increased, the FL peaks gradually decreased because of the loss of the quantum size effect induced by abnormal growth, as shown in Fig. 1(a) [15]. When the reaction time increased up to 5 min, the absorption peaks of the $CsPbBr_3$ NCs remained unchanged, as depicted in Fig. 1(b). After 5 min of reaction time, the absorption peaks for the $CsPbBr_3$ NCs became broader. The

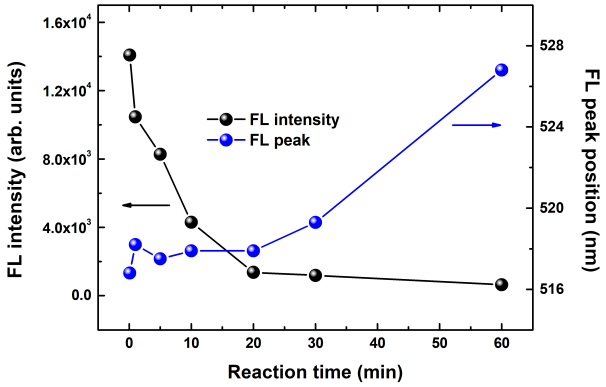

Figure 2. Fluorescence peak position and intensity of $CsPbBr_3$ nanocrystals as a function of reaction time.

intensity of the absorption spectra gradually decreased with increasing reaction time, suggesting a decrease in the light absorption capacity [16].

The variations of the FL peak position and intensity of the $CsPbBr_3$ NCs as a function of reaction time are displayed in Fig. 2. The FL peaks of as-obtained $CsPbBr_3$ perovskite NCs produced at reaction times of 5 s, 1, 5 , 10, 20, 30, and 60 min are located at 516.8, 518.2, 517.5, 517.9, 517.9, 519.3, and 526.8 nm, respectively. The redshift in the FL peaks of the $CsPbBr_3$ NCs with increasing reaction time is due to the ripening of $CsPbBr_3$ NCs [12,17]. The FL intensities decreased steadily, and the FL peaks nearly disappeared with increasing reaction time, as shown in Fig. 2, which can be attributed to the increased size of the $CsPbBr_3$ crystal. The $CsPbBr_3$ NCs were diluted with toluene solutions to give the same band edge optical density (0.05 at the respective band edge absorption peaks). The FL intensity of the $CsPbBr_3$ NC sample with a reaction time of 60 min decreased by nearly 20 times compared with that of the $CsPbBr_3$ NC sample with a reaction time of 5 s. These results are related to the induced charge trap states resulting from the surface decomposition reaction or the elimination of surface ligands [3].

Figure 3(a) shows the photoluminescence quantum yields (PLQYs) of the $CsPbBr_3$ NCs synthesized at a set reaction temperature (170 °C) and varying reaction times (5 s – 60 min). The relative PLQY of the $CsPbBr_3$ NCs were obtained by comparing the integrated emission of the $CsPbBr_3$ NC samples with a standard fluorescence dye (Coumarin 500 in ethanol, QY = 47%) [18]. The absorbance of the $CsPbBr_3$ NC samples was kept at less than 0.1 at 390 nm to prevent re-absorption [19]. The $CsPbBr_3$ NCs exhibited relative PLQYs (20–35%). The highest PLQY (35%) was attained for $CsPbBr_3$ NCs prepared at a reaction time of 5 s, and the overall PLQY decreased as the reaction time increased because of the change in size and morphology of $CsPbBr_3$ NCs [20]. Figures 3(b) and 3(c) show the digital photographs of the as-obtained $CsPbBr_3$ NCs prepared at various reaction times under white light and single 365 nm UV light source. PL quenching of the $CsPbBr_3$ NCs can be also observed with the naked eye under a UV light, as seen in Fig. 3(b). As the reaction time increased, the solution containing $CsPbBr_3$ NCs, with a yellow precipitate and colorless transparent supernatant, turned dark and became turbid. The initial light green color of $CsPbBr_3$ NCs turned to yellow phases with increasing reaction time, suggesting extensive precipitation of the $CsPbBr_3$ NCs prepared at high temperature as shown Fig. 3(c). The yellow phases are caused by large $CsPbBr_3$ crystal growth, and this phenomenon revealed a broader size distribution [3,16].

Figures 4(a) and 4(b) represent the low-magnification bright-field TEM image and selected-area diffraction (SAED) pattern of $CsPbBr_3$ NCs on the specific high temperature (≥130 °C) and reaction time (5 s). As shown in Fig. 4(a), almost all of the square-shaped $CsPbBr_3$ NCs uniformly formed at 170 °C, which is well-matched with already re-

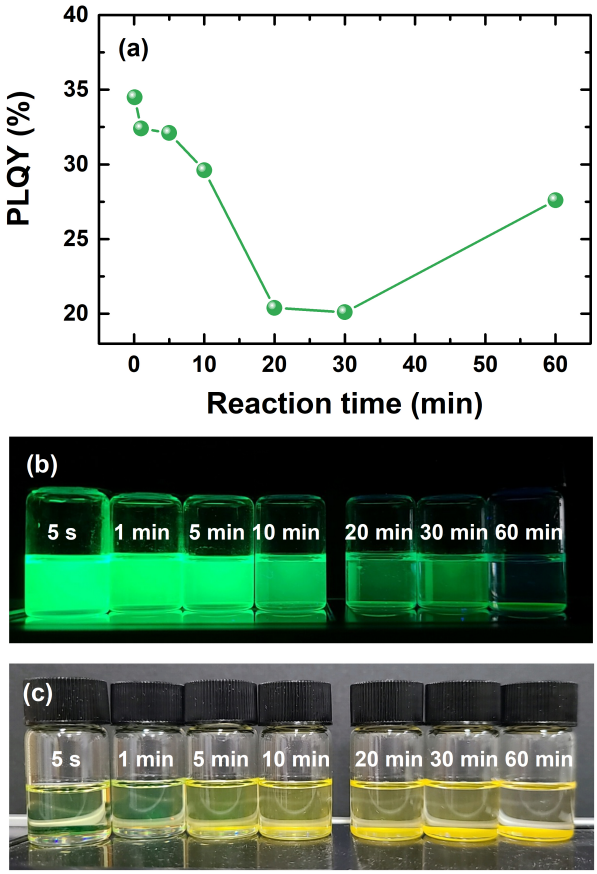

Figure 3. (a) Photoluminescence quantum yields of $CsPbBr_3$ nanocrystals as a function of reaction time. The digital photographs of the as-obtained $CsPbBr_3$ nanocrystals synthesized at various reaction time under (b) single 365 nm UV light and (c) white light.

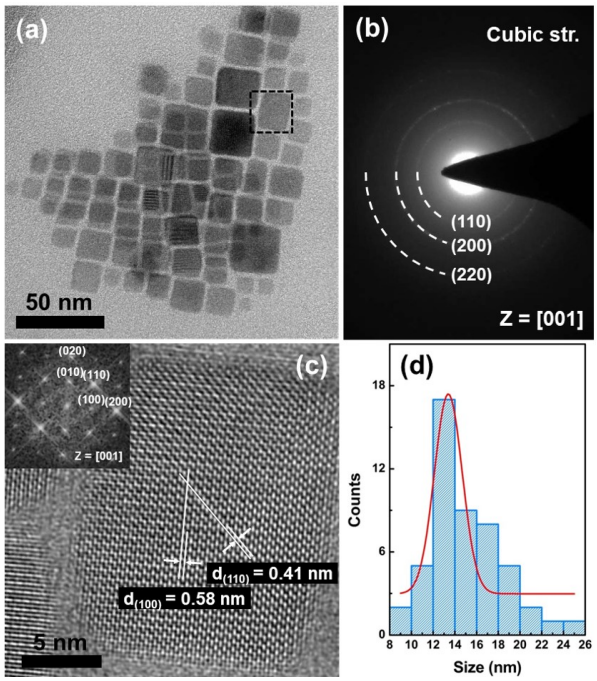

Figure 4. (a) Bright-field transmission electron microscopy image and (b) selected-area diffraction pattern of the $CsPbBr_3$ nanocrystals (170 °C, 5 s). (c) High-resolution transmission electron microscopy image from the black dotted box in (a) and the inset is a fast Fourier transform pattern of corresponding image. (d) Histogram of the size distribution of the $CsPbBr_3$ nanocrystals.

ported morphological characteristics of conventional colloidal $CsPbBr_3$ NCs [16,21]. The SAED ring pattern in Fig. 4(b) indicates that the lattice spacing of 0.41, 0.29, and 0.21 nm corresponds to the (110), (200), and (220) lattice planes, which agree well with the interplanar spacings of cubic-phase $CsPbBr_3$, respectively [22]. The nanostructural characteristics of the $CsPbBr_3$ NCs are also confirmed via the high-resolution TEM image depicted in Fig. 4(c) and fast Fourier transform pattern obtained from [001] beam direction (Z, zone axis). The lattice spacing of 0.41 and 0.58 nm corresponds to the (110) and (100) interplanar spacings of cubic-phase $CsPbBr_3$, respectively [22, 23]. The number of $CsPbBr_3$ NCs and size distributions is plotted with Gaussian distributions, as shown in Fig. 4(d), and the average size of the $CsPbBr_3$ NCs is 13.4 nm. The histogram of the particle size distribution for the $CsPbBr_3$ NCs was obtained by using ImageJ software [17, 24].

4. Conclusions

We investigated the influence of reaction time on the structural and optical properties of as-synthesized $CsPbBr_3$ perovskite NCs. The reaction conditions of $CsPbBr_3$ NCs can significantly affect the structure and crystal form of the NCs. The redshift of the FL wavelength and resultant decrease in the total absorption intensity with increasing reaction time was attributed to large $CsPbBr_3$ crystal growth by the ripening process. With increasing reaction time, the FL intensities and PLQYs gradually decreased because of the loss of quantum confinement and formation of charge trap states. TEM observations demonstrated that the $CsPbBr_3$ NCs with an initial reaction time of 5 s were well-crystallized in a cubic lattice. Our observations provide clear evidence that the $CsPbBr_3$ perovskite NCs are significantly affected by the reaction conditions, which can lead to significant changes in the particle morphology and associated optical properties. The results of this study suggest the importance of investigation of the optical properties in $CsPbBr_3$ NCs with various synthetic factors affecting the reliability and durability of optoelectronic devices.

Acknowledgements

This work was supported by the National Research Foundation of Korea (NRF) grant funded by the Korea government (MSIT) (NRF-2021R1A2C1003074).

Conflicts of Interest

The authors declare no conflicts of interest.

ORCID

Sung Hun Kim https://orcid.org/0000-0002-0792-4578
Yong-Ryun Jo https://orcid.org/0000-0002-7411-6132
Yong Bin Kim https://orcid.org/0000-0001-6720-2799
Ju Seok Kim https://orcid.org/0000-0002-8716-2904
Sang-Youp Yim https://orcid.org/0000-0001-5503-6957
Hong Seok Lee https://orcid.org/0000-0002-1292-0731

References

[1] H. Wang *et al.*, Nat. Commun. 10, 665 (2019).
[2] H. Yuan, Y. Zhao, J. Duan, Y. Wang, X. Yang, and Q. Tang, J. Mater. Chem. A 6, 24324 (2018).
[3] S. Huang, Z. Li, B. Wang, N. Zhu, C. Zhang, L. Kong, Q. Zhang, A. Shan, and L. Li, ACS Appl. Mater. Interfaces 9, 7249 (2017).

[4] P. Wang, N. Chai, C. Wang, J. Hua, F. Huang, Y. Peng, J. Zhong, Z. Ku, and Y.-b. Cheng, RSC Adv. 9, 11877 (2019).
[5] J. Chen, D. Liu, M. J. Al-Marri, L. Nuuttila, H. Lehtivuori, and K. Zheng, Sci. China Mater. 59, 719 (2016).
[6] G. Niu, X. Guo, and L. Wang, J. Mater. Chem. A 3, 8970 (2015).
[7] R. G. Niemann, L. Gouda, J. Hu, S. Tirosh, R. Gottesman, P. J. Cameron, and A. Zaban, J. Mater. Chem. A 4, 17819 (2016).
[8] E. Erol, O. Kıbrıslı, M. Ç. Ersundu, and A. E. Ersundu, Chem. Eng. J. 401, 126053 (2020).
[9] Z. Wang, Z. Shi, T. Li, Y. Chen, and W. Huang, Angew. Chem. Int. Ed. 56, 1190 (2017).
[10] P. Song, B. Qiao, D. Song, Z. Liang, D. Gao, J. Cao, Z. Shen, Z. Xu, and S. Zhao, J. Alloys Compd. 767, 98 (2018).
[11] J. Song, J. Li, X. Li, L. Xu, Y. Dong, and H. Zeng, Adv. Mater. 27, 7162 (2015).
[12] Y. Xu, S. Lou, C. Xia, T. Xuan, and H. Li, J. Lumin. 222, 117132 (2020).
[13] V. K. LaMer and R. H. Dinegar, J. Am. Chem. Soc. 72, 4847 (1950).
[14] X. Li, K. Zhang, J. Li, J. Chen, Y. Wu, K. Liu, J. Song, and H. Zeng, Adv. Mater. Interfaces 5, 1800010 (2018).
[15] T. Kosugi, Y. Iso, and T. Isobe, Chem. Lett. 48, 349 (2019).
[16] J. Lan, L. Luo, M. Wang, F. Li, X. Wu, and F. Wang, J. Lumin. 210, 464 (2019).
[17] M. Koolyk, D. Amgar, S. Aharon, and L. Etgar, Nanoscale 8, 6403 (2016).
[18] S. H. Kim, K.-D. Park, and H. S. Lee, Energies 14, 275 (2021).
[19] S. L. Hu, K. Y. Niu, J. Sun, J. Yang, N. Q. Zhao, and X. W. Du, J. Mater. Chem. 19, 484 (2009).
[20] C. Chen, L. Zhang, T. Shi, G. Liao, and Z. Tang, Nanomaterials 9, 1751 (2019).
[21] X. Zhang, B. Xu, J. Zhang, Y. Gao, Y. Zheng, K. Wang, and X. W. Sun, Adv. Funct. Mater. 26, 4595 (2016).
[22] M. Rodová, J. Brožek, K. Knížek, and K. Nitsch, J. Ther. Anal. Calorim. 71, 667 (2003).
[23] L. Yang, B. Fu, X. Li, H. Chen, and L. Li, J. Mater. Chem. C 9, 1983 (2021).
[24] S. H. Kim, M. T. Man, J. W. Lee, K.-D. Park, and H. S. Lee, Nanomaterials 10, 1589 (2020).